ESA Cloud_cci

Algorithm Theoretical Baseline Document v5.1

(Applicable to Cloud_cci version 2.0 products)

Issue 5 Revision 1

12 September 2017

Document Change Record

Document, Version	Date	Changes	Originator
ATBD Version 5.0	20/05/2017	- Initial version based on ATBD Version 4.0 - Changing name of document - Including note on Cloud_cci version 2.0 datasets and DOIs on front page - Updating project description in Section 1 (now identical to corresponding information in PUG and PVIR) - Aligning structure and layout with PUG and PVIR - Including information about SLSTR and OLCI sensors - Updating CC4CL and FAME-C descriptions	C. Carbajal Henken C. Poulsen M. Stengel
ATBD Version 5.1	04/07/2017	Minor modifications according to ESA review	M. Stengel

Purpose

The purpose of the Cloud_cci Algorithm Theoretical Baseline Documents (ATBDs) is to document the theoretical background of all components of the algorithms used for the generation of the Cloud_cci cloud property datasets v2.0. This document focusses on overarching aspects as individual, in-depth ATBDs exist for the two retrieval systems applied in Cloud_cci (Community Cloud retrieval for Climate – CC4CL, ATBD-CC4CLv5; Freie Universität Berlin AATSR MERIS Cloud retrieval - FAME-C, Carbajal Henken et al., 2014).

Table of Contents

1. Introduction

1.1 The ESA Cloud_cci project

The ESA Cloud_cci project covers the cloud component in the European Space Agency's (ESA) Climate Change Initiative (CCI) programme (Hollmann et al., 2013). In the ESA Cloud_cci project, long-term and coherent cloud property datasets have been generated exploiting the synergic capabilities of different Earth observation missions (European and non-European) allowing for improved accuracies and enhanced temporal and spatial sampling better than those provided by the single sources. The Cloud_cci datasets are the attempt to respond to GCOS requirements for the Cloud Properties Essential Climate Variable (ECV).
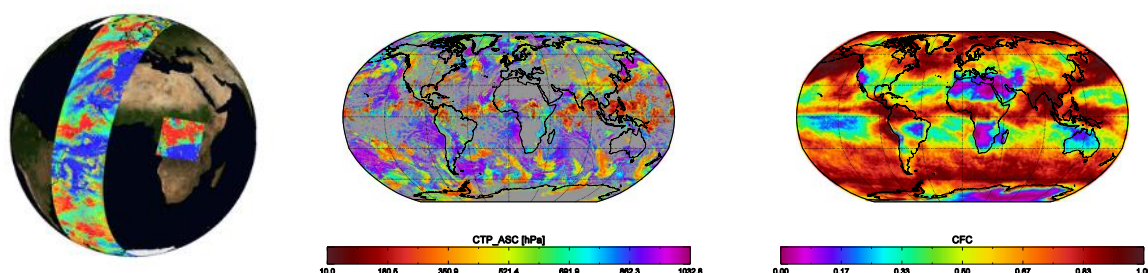

Figure 1-1 *Examples of Cloud_cci cloud products. Left: Pixel-based (Level 2), middle: daily composite on a global grid (Level 3U), right: monthly averaged on a global grid (Level 3C)*

To make the Cloud_cci datasets improved compared to existing ones, the following two essential steps were undertaken:

1) Revisit the measurement data (Level-1) and corresponding calibration performance and development of a carefully inter-calibrated and rigorously quality checked radiance data sets for AVHRR, so called Fundamental Climate Data Record (FCDR). Within this effort the calibration of AVHRR, MODIS and AATSR was compared and characterized. Please see the ATBDv5 for more information about all sensors used and their imaging characteristics. More information on the AVHRR FCDR produced and used is available in RAFCDRv1.0.

2) Development of two state-of-the-art physical retrieval systems that use the optimal estimation technique for a simultaneous, spectrally consistent retrieval of cloud properties including pixel-based uncertainty measures. The first retrieval framework is the Community Cloud retrieval for Climate (CC4CL; Sus et al., 2017; McGarragh et al., 2017) which is applied to AVHRR and AVHRR-heritage channels (i.e. channels which are available from all sensors) of MODIS and AATSR. The second retrieval framework is the Freie Universität Berlin AATSR MERIS Cloud retrieval (FAME-C; Carbajal Henken et al., 2014) and is applied to synergistic MERIS and AATSR measurements on-board of ENVISAT.

Based on these developments, six multi-annual, global datasets of cloud properties were generated using the passive imager satellite sensors AVHRR, MODIS, (A)ATSR and MERIS. These datasets were comprehensively evaluated (1) by using accurate reference observations of ground stations and space-based Lidar measurements and (2) by comparisons to existing and well-established global cloud property datasets.

All parts of the datasets generation effort were properly documented with the major components being the Product Validation and Intercomparisons Report (PVIR; PVIRv4.1), the Product User Guide (PUGv3.1) and this overarching Algorithm Theoretical Baseline Document (ATBD, ATBDv5) together with specific ATBDs for FAME-C (ATBD-FAME-Cv5) and CC4CL (ATBD-CC4CLv5).

Furthermore, to facilitate the utilization for evaluation of regional and global atmospheric models, the development of a satellite simulator package for Cloud_cci datasets were fostered, which is planned to be part of one of the upcoming releases of the CFMIP Observation Simulator Package (COSP, Bodas-Salcedo et al. 2011).

1.2 The Cloud_cci datasets

In Cloud_cci two families of global cloud property datasets have been generated. The first family comprises datasets for individual sensor groups such as AVHRR, MODIS, ATSR2/AATSR, for which the AVHRR-heritage channels (0.6, 0.8, 1.6/3.7, 10.8, 12.0 μm) were utilized to retrieve cloud properties using the CC4CL algorithm. The second family comprises a dataset of cloud properties retrieved from simultaneous usage of AATSR and MERIS sensors (both mounted on ENVISAT) by applying the FAME-C algorithm. Since MODIS and AVHRR sensors are separated into morning and afternoon orbits, 6 distinct Cloud_cci datasets exist, which can be seen in Figure 1-2. In addition,

Table 1-1 summarizes the algorithms, sensors and satellites used for each dataset. The official versions of the datasets, as released under the issued Digital Object Identifies (DOIs, see Table 1-2), do not contain any diurnal cycle or satellite drift correction. Potential methods for such a drift correction were investigated for AVHRR and were documented in RODCv1.0. In Figure 1-3 the local observation time of each individual sensor considered are visualized. This information is often essential for properly characterizing time series of cloud properties derived from the satellite-based climate datasets. Other important aspects are the imaging properties. The sensors differ in terms of native footprint resolution (1x1km² for ATSR2, AATSR, MERIS, MODIS; 5x1km² for AVHRR). This, together with the sensor swath width, lead to very different observation frequency and spatial coverage.. While MODIS and AVHRR have a complete global coverage within a day, the AATSR sensor needs about 3 days to accomplish this, however, with a higher spatial resolution compared to AVHRR.
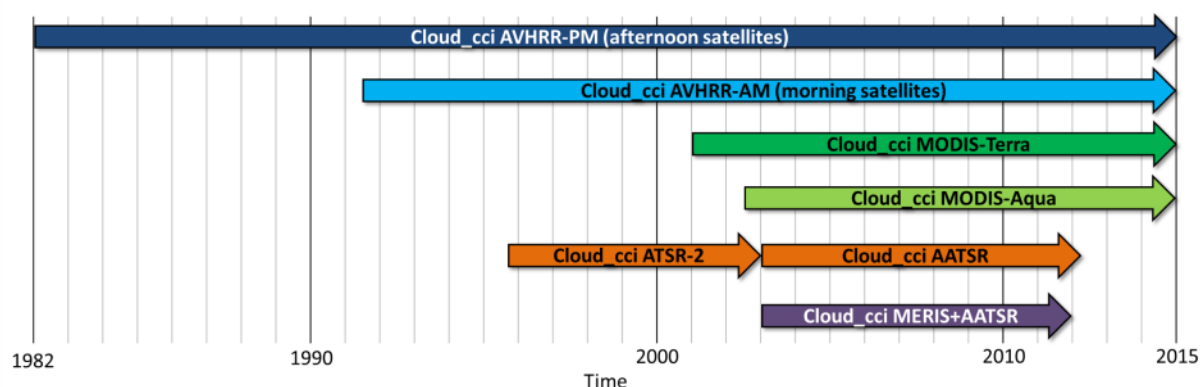
Figure 1-2 *Overview of Cloud_cci datasets and the time periods they cover.*

All datasets contain identical sets of cloud properties: cloud mask/fraction (CMA/CFC), cloud phase/liquid cloud fraction (CPH), cloud top pressure/height/temperature (CTP/CTH/CTT), cloud effective radius (CER), cloud optical thickness (COT), spectral cloud albedo at two wave lengths (CLA) and liquid/ice water path (LWP/IWP). The data is presented at different processing levels ranging from pixel-based retrieval products (Level-2), which are additionally projected (sampling – no averaging) onto a global Latitude-Longitude grid of 0.05° resolution (global composite, Level-3U), to monthly data summarizes including averages, standard deviation and histograms - all defined on a global Latitude-Longitude grid of 0.5° resolution (Level-3C). See Section 1.3 for more details.

All cloud properties (except CPH) are accompanied by uncertainty measures at all processing levels, which range from optimal estimation based uncertainty on pixel level (Level-2 and Level-3U) to propagated uncertainties in the monthly Level-3C products. See Section 1.2 for more information.

In addition to the passive imager based datasets mentioned so far, in Cloud_cci an IASI-based demonstrator dataset has been created, with more details to be found in Feofilov et al. (2017) and Stubenrauch et al. (2017).

Key strengths of Cloud_cci datasets:

- The Cloud_cci datasets are based on two newly-developed, state-of-the art retrieval systems named CC4CL and FAME-C that use the optimal estimation (OE) technique and are applied to passive imager sensors of current and past European and non-European satellite missions.

- The measurement records of the utilized sensors have been revisited, re-characterized and, in case of AVHRR, re-calibrated.

- Two special features of CC4CL and FAME-C are, among others, their applicability to multiple sensors: ATSR2, AATSR, MODIS, AVHRR (CC4CL) and the simultaneous utilization of AATSR and MERIS measurements (FAME-C, i.e. utilizing the O2-A band of MERIS) down to spatial footprint resolutions of 1km.

- Radiative consistency of derived cloud parameters is achieved by the OE-based, iterative fitting of a physically consistent cloud model (and radiative transfer simulations therefrom) to the sensor measurements in the visible and thermal infrared spectral range.

- Pixel-level uncertainty characterization is facilitated by the OE technique, which is physically consistent (1) with the uncertainties of the input data (e.g. measurements, a-priori) and (2) among the retrieved variables. These pixel-level uncertainties are further propagated into the monthly products using a developed sound mathematical framework.

- Potential to combine AVHRR-heritage datasets to achieve increased temporal resolution by including multiple polar-orbiting satellite instruments, which also allows for mature cloud property histograms on 0.5° resolution due to highly increased sampling rate.

- Comprehensive assessment and documentation of the retrieval schemes and the derived cloud property datasets, including possibilities of drift- and diurnal cycle corrections.

- Availability of a developed Cloud_cci satellite simulator facilitating the applicability of Cloud_cci data in regional and global climate models evaluation efforts.

- All datasets are available in netcdf (v4) format and fulfil high CCI-internal and external data standards (e.g. Climate and Forecast – CF conventions).

- The datasets have been submitted for inclusion in the obs4MIPs database for use in CMIP model intercomparison and verification studies.

Table 1-1 *Cloud_cci datasets with the algorithms, sensor(s) and satellite(s) used and the time periods they cover. The Digital Object Identifiers (DOI) of all datasets are also listed.*

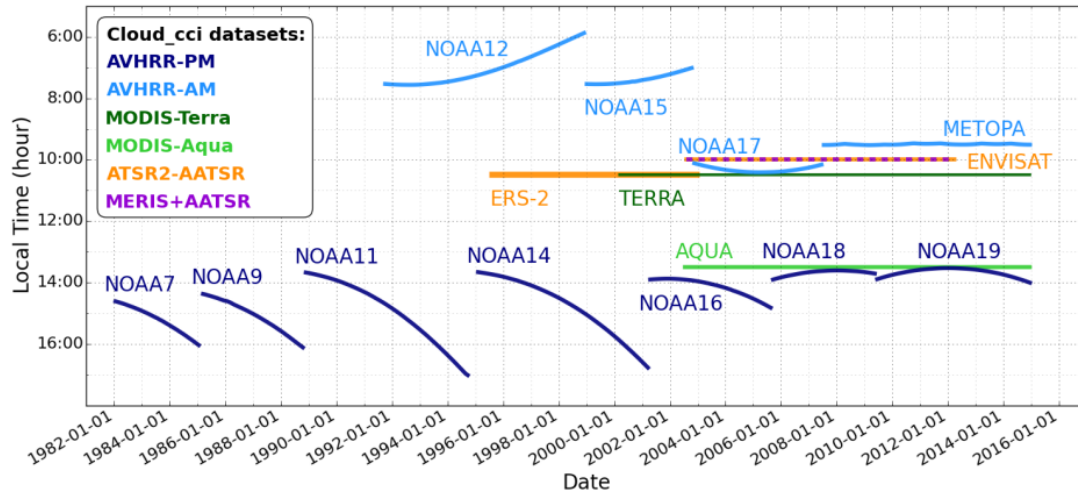| Dataset name	Sensor(s)	Satellite(s)	Time period	Algorithm
Cloud_cci AVHRR-PM DOI:10.5676/DWD/ESA_Cloud_cci/AVHRR-PM/V002	AVHRR-2/-3	NOAA-7,-9,-11,-14,-16,-18,-19	1982-2014	CC4CL
Cloud_cci AVHRR-AM DOI:10.5676/DWD/ESA_Cloud_cci/AVHRR-AM/V002	AVHRR-2/-3	NOAA-12,-15,-17, Metop-A	1991-2014	CC4CL
Cloud_cci MODIS-Terra DOI:10.5676/DWD/ESA_Cloud_cci/MODIS-Terra/V002	MODIS	Terra	2000-2014	CC4CL
Cloud_cci MODIS-Aqua DOI:10.5676/DWD/ESA_Cloud_cci/MODIS-Aqua/V002	MODIS	Aqua	2002-2014	CC4CL
Cloud_cci ATSR2-AATSR DOI:10.5676/DWD/ESA_Cloud_cci/ATSR2-AATSR/V002	ATSR2, AATSR	ERS2, ENVISAT	1995-2012	CC4CL
Cloud_cci MERIS+AATSR DOI:10.5676/DWD/ESA_Cloud_cci/MERIS+AATSR/V002	MERIS, AATSR	ENVISAT	2003-2011	FAME-C

Figure 1-3 *Time periods and local observation times (equator crossing times) of each satellite sensor considered in Cloud_cci. Figure is taken from Stengel et al. (2017).*

1.3 Cloud_cci cloud products

The cloud properties derived on pixel level of each utilized sensor are listed in Table 1-2. It is important to note that the properties CLA, LWP, IWP are not directly retrieved, but rather determined from retrieved COT and CER in a post processing step. The same applies to CTH and CTT, which are inferred from the retrieved CTP. Based on these pixel level retrievals the data is further processed into different processing levels as summarized in Table 1-3. Level-3U denotes a composite on a global Latitude-Longitude grid (of 0.05° resolution) onto which the Level-2 data is sampled (see ATBDv5 for more details on Level-3U sampling). Level-3C products are also defined on Latitude-Longitude grid (here 0.5° resolution) onto which the properties are averaged or their frequency collected (histograms). Further separation of cloud properties in Level-3C in e.g. day/night, liquid/ice, were made wherever suitable (see Table 1-4). Level-3S products are generated merging the Level-3C of all individual sensors. Using Level-3S products requires careful consideration of the partly large and time-varying discrepancies between the used sensors. For this reason Level-3S data is only available upon specific request. Please contact the Cloud_cci team for more information (http://www.esa-cloud-cci.org/?q=support).

Table 1-2 *List of generated cloud properties. CMA/CFC and CPH are derived in a pre-processing step. In the next step, COT, CER and CTP are retrieved simultaneously by fitting a physically consistent cloud/atmosphere/surface model to the satellite observations using optimal estimation (OE). Moreover, LWP and IWP are obtained from COT and CER. In addition, spectral cloud albedo (CLA) for two visible channels are derived.*

Variable	Abbrev.	Definition
Cloud mask / Cloud fraction	CMA/ CFC	A binary cloud mask per pixel (L2, L3U) and therefrom derived monthly total cloud fractional coverage (L3C, L3S) and separation into 3 vertical classes (high, mid-level, low clouds) following ISCCP classification (Rossow and Schiffer, 1999).
Cloud phase	CPH	The thermodynamic phase of the retrieved cloud (binary: liquid or ice; in L2, L3U) and the therefrom derived

Variable	Abbrev.	Definition
		monthly liquid cloud fraction (L3C, L3S).
Cloud optical thickness	COT	The line integral of the absorption coefficient and the scattering coefficient (at 0.55µm wavelength) along the vertical in cloudy pixels.
Cloud effective radius	CER	The area-weighted radius of the cloud drop and crystal particles, respectively.
Cloud top pressure/ height/ temperature	CTP/ CTH/ CTT	The air pressure [hPa] /height [m] /temperature [K] of the uppermost cloud layer that could be identified by the retrieval system.
Cloud liquid water path/ Ice water path	LWP/ IWP	The vertical integrated liquid/ice water content of existing cloud layers; derived from CER and COT. LWP and IWP together represent the cloud water path (CWP)
Joint cloud property histogram	JCH	This product is a spatially resolved two-dimensional histogram of combinations of COT and CTP for each spatial grid box.
Spectral cloud albedo	CLA	The blacksky cloud albedo derived for channel 1 (0.67 µm) and 2 (0.87 µm), respectively (experimental product)
Cloud effective emissivity	CEE	cloud radiative thickness in the infrared typically referred to as the "effective emissivity"

Table 1-3 *Processing levels of Cloud_cci data products. Level-3U, Level-3C and Level-3S are each directly derived from Level-2.*

Processing level	Spatial resolution	Description
Level-2 (L2)	MODIS: 1km AATSR: 1km AVHRR: 5 km MERIS+ AATSR: 1km	Retrieved cloud variables at satellite sensor pixel level, thus with the same resolution and location as the sensor measurements (Level-1)
Level-3U (L3U)	Latitude-Longitude grid at 0.05° res. (MODIS-Europe: 0.02°)	Cloud properties of Level-2 orbits projected onto a global space grid without combining any observations of overlapping orbits. Only subsampling is done. Common notation for this processing level is also L2b. Temporal coverage is 24 hours (0-23:59 UTC).
Level-3C (L3C)	Latitude-Longitude grid at 0.5° res.	Cloud properties of Level-2 orbits of one single sensor combined (averaged / sampled for histograms) on a global space grid. Temporal coverage of this product is 1 month.
Level-3S (L3S)	Latitude-Longitude grid at 0.5° res.	Cloud properties of Level-2 orbits of all available single sensors combined (averaged / sampled for histograms) on a global space grid. Temporal coverage of this product is 1 month.

Table 1-4 *Cloud_cci product features incl. day and night separation, liquid water and ice as well as histogram representation. Level-3U refers to the non averaged, pixel-based cloud retrievals sampled onto a global Latitude-Longitude (lat/lon) grid. [1]CMA in Level-2 and Level-3U is a binary cloud mask. All products listed exist in each dataset listed above.*

	Level 2 swath based 1km/5km	Level-3U daily sampled global 0.05° lat/lon grid	Level-3C monthly averages global 0.5° lat/lon grid	Level-3C monthly histograms global 0.5° lat/lon grid
CMA/CFC	✔ as CMA[1]	✔ as CMA[1]	✔day/night/high/mid/low	-
CTP, CTH, CTT	✔	✔	✔	✔ liquid/ice
CPH	✔	✔	✔ day/night	-
COT	✔	✔	✔ liquid/ice	✔ liquid/ice
CER	✔	✔	✔ liquid/ice	✔ liquid/ice
LWP	✔ as CWP	✔ as CWP	✔	✔ as CWP
IWP			✔	
CLA	✔ 0.6/0.8µm	✔ 0.6/0.8µm	✔ 0.6/0.8µm	✔ 0.6/0.8µm/liquid/ice
JCH	-	-	-	✔ liquid/ice

2. Satellite sensors and their measurement records

An important aspect for any product-based climate dataset (formally denoted Thematic Climate Data Records – TCDRs) is that retrieved products have been derived from accurately calibrated and homogenized radiances (formally denoted Fundamental Climate Data Records – FCDRs). In the ESA Cloud_cci Phase 1, studies were made to evaluate currently available Level 1 datasets. These studies concentrated on the first product demonstration period 2007-2009.

In the ESA Cloud_cci Phase 2, processing of a much longer time period were carried out: > 30 years for AVHRR, > 10 years for MODIS data and 10 years for AATSR and MERIS data. In the following sections we describe which Level 1 were used and how these datasets were prepared (if applicable). Figure 1-3 gives an overview of all sensors (and their time periods) used in Cloud_cci.

2.1 AVHRR

Sensor characteristics

Measurements from the Advanced Very High Resolution Radiometer (AVHRR) radiometer on board the polar orbiting NOAA satellites and the EUMETSAT MetOp satellites have been performed since 1978. The instrument only measured in four spectral bands in the beginning (AVHRR/1), but from 1982 a fifth channel was added (AVHRR/2) and in 1998 even a sixth channel (1.6 *μm*)was made available (AVHRR/3), although only accessible if switched with the previous third channel at 3.7 *μm*.

Table 2-1 describes the AVHRR instrument, its various versions and the satellites carrying them. The AVHRR instrument measures at a horizontal resolution close to 1 km at nadir but only data at a reduced resolution of approximately 4 km are permanently archived and available with global coverage since the beginning of measurements. This dataset is denoted Global Area Coverage (GAC) AVHRR data. See Figure 2-1 for a schematic description of the GAC generation.

Table 2-1 *Spectral channels of the Advanced Very High Resolution Radiometer (AVHRR). The three different versions of the instrument are described as well as the corresponding satellites. Notice that channel 3A was only used continuously on NOAA-17 and Metop-A. For the other satellites carrying AVHRR/3, channel 3A was used only for shorter periods.*

Channel Number	Wavelength (μm) AVHRR/1 NOAA-6,8,10	Wavelength (μm) AVHRR/2 NOAA-7,9,11,12,14	Wavelength (μm) AVHRR/3 NOAA-15,16,17,18 NOAA-19, Metop-A
1	0.58-0.68	0.58-0.68	0.58-0.68
2	0.725-1.10	0.725-1.10	0.725-1.10
3A	-	-	1.58-1.64
3B	3.55-3.93	3.55-3.93	3.55-3.93
4	10.50-11.50	10.50-11.50	10.50-11.50
5	Channel 4 repeated	11.5-12.5	11.5-12.5

AVHRR data record used in Cloud_cci

As a baseline for Cloud ECV production in Phase 2 the calibration work of NOAA (Heidinger et al., 2010) was used, which corrects the visible and 1.6 µm channels of AVHRR. The calibration was updated based on an improved calibration reference in MODIS Collection 6 (Heidinger, 2014, personal communication). This update was the basis for the production of an (intermediate) FCDR which was used in Cloud_cci for the production of the AVHRR-based ECV datasets. The calibration of infrared AVHRR channels is basically left untouched since on-board blackbody calibration targets were found to provide stable and reliable results. However, for future upgrades of the AVHRR FCDR remaining issues with the infrared channels (e.g., see Mittaz and Harris (2009)) need to be addressed.
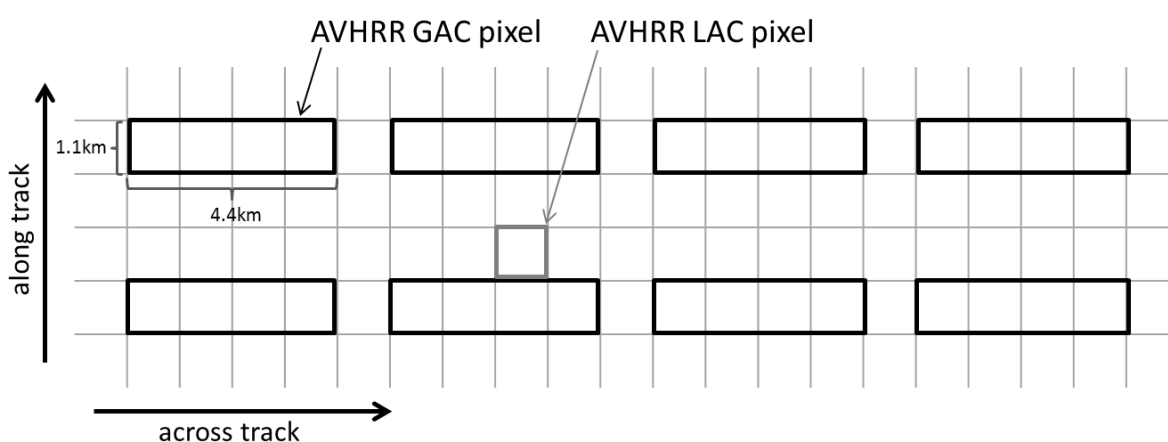

Figure 2-1 *Schematic view on the conversion of original AVHRR 1 km pixel (Local area coverage – LAC) data to the GAC format.*

The upgraded calibration and inter-calibration is realised through the use of a new pre-processing module, denoted PyGAC. PyGAC is an open-source community-driven Python interface to read and calibrate raw level 1b AVHRR GAC data. PyGAC takes advantage of the modular and object oriented philosophy of the Python programming language and its vast cache of public utilities.

For each AVHRR GAC orbit, PyGAC provides calibrated reflectances and brightness temperatures, sun and satellite zenith and azimuth angles and scanline quality information. The output files have HDF5 and netCDF formats and follow international Climate and Forecast conventions. In addition to calibration improvements, also the geolocation is improved for the historical part of AVHRR data (second generation, AVHRR/2) using clock-drift corrections provided by the University of Miami. The PyGAC interface is easily adaptable to be able to compute independent navigation information. A publication describing PyGAC in more details is under preparation. Most important aspects of this task are also documented in RAFCDRv1.0.

For potential future application of the AVHRR Level-1 data, it is the ambition to take on board potential improvements resulting from the WMO Space Programme activity "Advancing the AVHRR FCDR) coordinated by the SCOPE-CM (Sustained, Coordinated Processing of Environmental Satellite Data for Climate Monitoring) programme. As a further complement to these calibration improvements, also navigation corrections will have to be improved for some of the early afternoon satellites utilising pre-existing information on clock errors.

2.2 MODIS

Sensor characteristics

MODIS (Moderate Resolution Imaging Spectroradiometer) is an advanced imaging instrument on board the Terra (EOS AM) and Aqua (EOS PM) polar satellites (see http://modis-atmos.gsfc.nasa.gov/index.html). Terra's orbit around the Earth is sun synchronous and timed so that it crosses the equator from north to south in the morning (local solar time 10:30), while Aqua crosses the equator from south to north in the afternoon (local solar time 13:30) (see Figure 1-3). Terra MODIS and Aqua MODIS are viewing the entire Earth's surface every 1 to 2 days, acquiring data in 36 spectral bands or groups of wavelengths (see Table 2-2).

MODIS data record used in Cloud_cci

The MODIS L1b Collection 6 data were directly retrieved from NASA. They were based on the NASA MODIS collection 6 processing, followed by a post-processing, which performed a selection of a subset of 6 of the 36 channels. The data were afterwards transferred to ECMWF computer facilities.

The MODIS instruments have a sophisticated on-orbit calibration approach including radiometric, spatial, and spectral on-board calibrators and the Moon as reference. MODIS instruments are well known for their high calibration accuracy. The Collection 6 Level 1 data are expected to show several improvements over Collection 5 data due to improved calibration methodologies. As a result, for the short-wave channels a long-term drift was removed and for the long-wave channels updated calibration coefficients were derived. Furthermore, the uncertainty information for all channels was updated. More details about all improvements of Collection 6 data can be found at: http://mcst.gsfc.nasa.gov/calibration/collection_6_info.

Table 2-2 *Spectral properties of the MODIS bands (information taken from http://modis.gsfc.nasa.gov/about/specifications.php).*

Band	Bandwidth[1]	Spectral Radiance[2]	Required SNR[3]	Band	Bandwidth[1]	Spectral Radiance[2]	Required SNR[3]
1*	620 - 670	21.8	128	20*	3.660 - 3.840	0.45(300K)	0.05
2*	841 - 876	24.7	201	21	3.929 - 3.989	2.38(335K)	2.00
3	459 - 479	35.3	243	22	3.929 - 3.989	0.67(300K)	0.07
4	545 - 565	29.0	228	23	4.020 - 4.080	0.79(300K)	0.07
5	1230 - 1250	5.4	74	24	4.433 - 4.498	0.17(250K)	0.25
6	1628 - 1652	7.3	275	25	4.482 - 4.549	0.59(275K)	0.25
7	2105 - 2155	1.0	110	26	1.360 - 1.390	6.00	150(SNR)
8	405 - 420	44.9	880	27	6.535 - 6.895	1.16(240K)	0.25
9	438 - 448	41.9	838	28	7.175 - 7.475	2.18(250K)	0.25
10	483 - 493	32.1	802	29	8.400 - 8.700	9.58(300K)	0.05
11	526 - 536	27.9	754	30	9.580 - 9.880	3.69(250K)	0.25

12	546 - 556	21.0	750
13	662 - 672	9.5	910
14	673 - 683	8.7	1087
15	743 - 753	10.2	586
16	862 - 877	6.2	516
17	890 - 920	10.0	167
18	931 - 941	3.6	57
19	915 - 965	15.0	250

31*	10.780 - 11.280	9.55(300K)	0.05
32*	11.770 - 12.270	8.94(300K)	0.05
33	13.185 - 13.485	4.52(260K)	0.25
34	13.485 - 13.785	3.76(250K)	0.25
35	13.785 - 14.085	3.11(240K)	0.25
36	14.085 - 14.385	2.08(220K)	0.35

[1] Bands 1 to 19 are in nm; Bands 20 to 36 are in µm
[2] Spectral Radiance values are (W/m^2 -µm-sr)
[3] SNR = Signal-to-noise ratio
[4] NE(delta)T = Noise-equiv. temperature difference
* AVHRR-heritage channels of MODIS used in CC4CL

2.3 AATSR

Sensor characteristics

AATSR has seven spectral bands in the solar, near-infrared and infrared range between 0.55 µm and 12 µm. It scans the Earth's surface with a conically scanning mirror directing radiation from two apertures onto the radiometer. This enables the instrument to view the Earth at two different angles, the nadir view and the forward view at an angle of 55° from the nadir. At nadir the pixel resolution is approximately 1x1 km^2 with a swath width of 512 pixels. The instrument is designed to be self-calibrating, with two integrated thermally controlled black-body targets for calibration of the thermal channels as well as an opal visible calibration target, which is illuminated by sunlight, for the visible/near-infrared channels. Central wavelengths and bandwidths of each AATSR channel are given in Table 2-3.

Table 2-3 *AATSR spectral channels*

Channel	Wavelength [nm]	Bandwidth [nm]
1	550	20
2*	665	20
3*	865	20
4	1610	60
5*	3740	380
6*	10850	900
7*	12000	1000

* AVHRR-heritage channels of AATSR used in CC4CL

ATSR-2/AATSR data record used in Cloud_cci

The ATSRs are designed to have exceptional long term sensitivity and stability of calibration. Thermal channels are calibrated using two on board black bodies at known temperatures which are observed during each across-track scan of the instrument. This makes it possible to determine single channel equivalent brightness temperatures correct to 0.05K (Smith et al., 2001). The instrument also has an on board visible/near-infrared calibration system enabling the visible channels to be

calibrated to an accuracy of better than 4% (Smith et al., 2008), which is subsequently improved via vicarious calibration using scenes of known stable surface BRDF (certain deserts and ice caps).

The vicarious calibration must be applied to the ATSR and AATSR level1b visible channel data before level2 data processing can begin. The vicarious calibration correction is updated regularly and can be accessed at http://www.aatsrops.rl.ac.uk/EDSX/OtherInfo/.

Complementary to the vicarious calibration based on surface reference sites, inter-comparisons between Aqua-MODIS and AATSR radiances (with previous vicarious calibration corrections applied) were performed using the SNO approach. Because of the orbit differences of ENVISAT and Aqua, SNOs were only possible at latitudes close to 70°N and 70°S. Figure 2-2 below shows results for the AATSR AVHRR-heritage channels at 665 nm, 865 nm and 1610 nm. Note that results are based exclusively on SNO targets matching the criteria of being well-illuminated (i.e., having solar zenith angles below 70°), not too dark (i.e, reflectance factors above 10 %) and homogeneous (i.e., internal reflectance standard deviation less than 1 %). Table 2-4 summarises SNO results for all channels (including also infrared channels at 3.7, 10.8 and 12.0 microns).
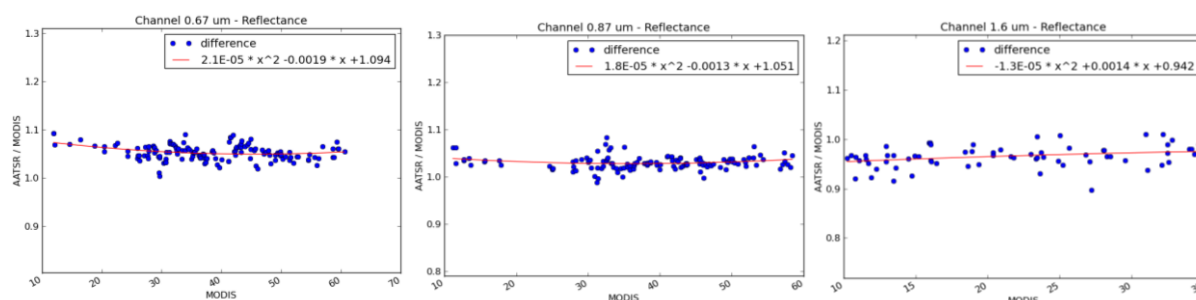

Figure 2-2 *AATSR reflectance factor quotas with respect to MODIS at 0.67 micron (a), 0.87 micron (b), 1.6 micron (c) for SNO targets collected in the period 2007-2009. Results are from Karlsson and Johansson (2014).*

Table 2-4 *Reflectance factor quota (AATSR/MODIS) or brightness temperature quota with respect to MODIS-Aqua deduced from SNO inter-comparisons in the period 2007-2009. Results are from Karlsson and Johansson (2014).*

AATSR channel	Wavelength [nm]	Reflectance factor quota or Brightness temperature quota
1	550	n.a.
2	665	1.050
3	865	1.029
4	1610	0.965
5	3740	1.000
6	10850	1.000
7	12000	0.999

Results show higher AATSR reflectances (5.0 % and 2.9 %, respectively) for channels 2 and 3 but about 3.5 % lower reflectances in channel 4 than MODIS. No trend was indicated for channels 2 and 3 but a slightly increasing AATSR trend (i.e., decreasing difference compared to MODIS) was noticed for channel 4. For infrared channels, the agreement appears to be very good.

Deviations for two of the visible channels can be compared to Figure 2-3 showing corresponding results over surface reference sites as presented by Bouvet et al. (2012). Here, measured

reflectances have been compared to modelled radiances for the surface sites collected during approximately the same time period (2006-2009). We notice a relative difference between AATSR and MODIS reflectances of approximately 3 % at 660 nm and 4 % at 870 nm. This agrees reasonably well with results presented in Table 2-4.

The nature of the differences found for the visible channels still remains to be not fully understood. However, studies of the influence of various spectral variations of the surface site reflectance and the atmosphere (transferred via different spectral response functions – elaborated in further detail in Bouvet et al., 2012) indicate that this can explain most of the difference. Thus, inter-comparison methods must be able to compensate better for these effects before firm conclusions about any remaining calibration biases can be made and further applied in calibration correction methods. Consequently, it was decided to stay with the current AATSR calibration based on vicarious calibration from surface sites for cloud products generated for the period 2007-2009.
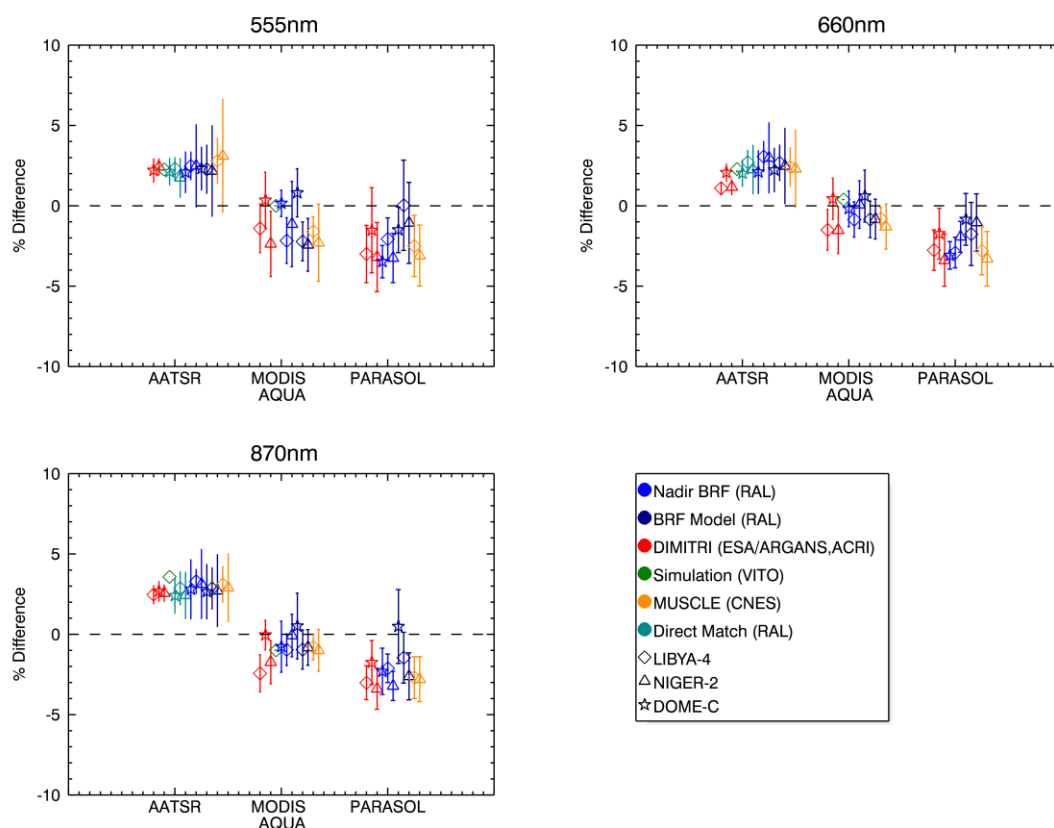
Figure 2-3 *Intercomparisons using direct matchups, nadir BRF and full BRF model including a correction for systematic uncertainties. Error bars represent the k=1 standard deviation of the differences between the measurements and reference (from Bouvet et al., 2012).*

2.4 SLSTR

Sensor characteristics

The SLSTR (Sea and Land Surface Temperature Radiometer) sensor is a 11-channel passive imaging sensor with dual viewing directions for accurate atmospheric corrections. SLSRT channels are spectrally located between 0.55 and 12.00 µm. Focus of SLSTR is multi-purpose VIS/IR imagery, with emphasis for example on surface temperature and cloud property retrievals. Precursor sensors are ATSR. ATSR2 and AATSR on board ERA, ERS-2 and Envisat. SLSTR is a payload of the Sentinel-3

satellite which was launched in February 2016. SLSTR swath with is 1400 km for cross-nadir and 740 km for aft-viewing swath. Spatial footprint size of one pixel is 0.5 km for short-wave channels and 1.0 km for IR channels. Table 2-3 lists the SLSTR channels.

Table 2-5 *SLSTR spectral channels*

Channel	Wavelength [nm]	Bandwidth [nm]
1	550	20
2*	665	20
3*	865	20
4	1375	
5	1610	60
6	2250	
7*	3740	380
8*	10850	900
9*	12000	1000

* AVHRR-heritage channels of SLSTR used in CC4CL

SLSTR data record used in Cloud_cci

Level 1b data of SLSTR is used in Cloud_cci. Data identifier: SL1_RBT at Near Real Time (NRT).

2.5   MERIS

Sensor characteristics

Within the FAME-C algorithm, AATSR measurements are synergistically combined with measurements of the Medium Resolution Imaging Spectrometer (MERIS). Both MERIS and AATSR are mounted on the ESA polar orbiting satellite ENVISAT, which was launched in 2002 and flies at 800 km altitude in a sun-synchronous orbit with an equator crossing time of 10.30 AM, descending node, and 98.5° inclination.

MERIS has fifteen spectral bands in the solar spectral range between 400 nm and 900 nm, as listed in Table 2-6. The instrument scans the Earth's surface using the pushbroom method. The CCD array provides spatial sampling in the across track direction, while the satellite's motion provides scanning in the along-track direction. The instrument has a field of view of 68.5°, shared by five identical cameras arranged in a fan shape configuration, and a swath width of 1150 km. The Earth is imaged with a spatial resolution of 1200x1000 m^2 in the reduced resolution mode. On-board calibration of MERIS is performed at the orbital South Pole, where the calibration diffuser is illuminated by the Sun by rotating a calibration mechanism.

Within FAME-C, all spectral channels of MERIS are used for cloud detection (in combination with the AATSR channels), and channels 10 and 11 are also used for the retrieval of cloud-top pressure.

Table 2-6 *MERIS spectral channels*

Channel	Wavelength [nm]	Bandwidth [nm]
1	412.5	10
2	442.5	10
3	490	10
4	510	10
5	560	10
6	620	10
7	665	10
8	681.2	7.5
9	708.75	10

Channel	Wavelength [nm]	Bandwidth [nm]
10*	753.75	7.5
11*	761.75	3.75
12	778	15
13	865	20
14	885	10
15	900	10

* MERIS channels used in FAME-C

MERIS data record used in Cloud_cci

MERIS has onboard calibration devices that are used routinely for radiometric and spectral calibration of the instrument. Within Cloud_cci, L1b data of the 3rd reprocessing of the MERIS archive are used.

The radiometric gain calibration of MERIS is performed with respect to the sun. A sun-illuminated white diffuser plate is inserted into the field of view of MERIS at the cross-over point of the five cameras' fields of view. The diffuser provides a reflectance standard across the entire spectral range and field of view. In this way a full aperture instrument calibration which follows the same optical path as in the observation modes is realized. The signal, averaged over a sufficiently large number of frames, is then divided by the BRDF of the diffuser obtained from pre-flight, on-ground characterization, yielding the absolute radiometric gains.

The white diffuser plate was exposed to the sun repeatedly during the course of the MERIS mission. Therefore, a limited degradation of the diffuser plate reflectivity was expected, caused by this radiation exposure. A second diffuser is therefore provided to evaluate changes in the BRDF of the commonly used diffuser. This diffuser is used infrequently and thus does not degrade as quickly as the first diffuser. In doing so, the stability of the gain calibration is assured for the whole MERIS lifetime.

The MERIS spectral calibration is achieved by inserting a wavelength diffuser into the field of view of MERIS, featuring well-characterized absorption minima. For this purpose, MERIS is reprogrammed to sample adequately these absorption features. As a result, the spectral distribution law is obtained, which relates spectral bands to their central wavelengths. As an alternative, the solar Fraunhofer lines, seen when observing the radiometric diffuser, are used for spectral calibration. Since the operational spectral calibration procedures are known to work less satisfactorily for the oxygen A band channel of MERIS, empirically determined central wavelengths for this band are used, adopted from Lindstrot et al, 2010. Simultaneously, the band is corrected for instrumental stray light. This correction procedure reduces the so-called MERIS camera effects, that would result in camera-to-camera offsets in derived pressure products.

Inter-comparisons between Aqua-MODIS and MERIS radiances were performed using the SNO approach. Because of the orbit differences of ENVISAT SNOs were only possible at latitudes close to 70°N and 70°S. However, in practice only the SNOs in the northern hemisphere were accessible because of too high solar zenith angles for the Antarctic SNOs (i.e., available MERIS data were restricted to solar zenith angles well below the angles valid at the SNOs). Table 2-7 summarizes SNO results for the two investigated MERIS channels. Some deviations (i.e., lower MERIS radiances) were found, but because of the short duration of the investigated period and the restrictions on available SNOs from the southern hemisphere no firm conclusions could be made at this stage.

Table 2-7 *Radiance factor quota (MERIS/MODIS) with respect to MODIS deduced from SNO inter-comparisons in the period 2007-2009. Results are from Karlsson and Johansson (2014).*

MERIS channel	Wavelength [nm]	Radiance quota
7	665	0.983
13	865	0.971

2.6 OLCI

Sensor characteristics

The Ocean and Land Colour Instrument (OLCI) is the successor of MERIS and is mounted on board the polar-orbiting satellite Sentinel-3, which was launched in February 2016 (Donlon et al, 2012). OLCI has a slightly larger swath width than MERIS of 1270 km and a spatial resolution at nadir of about 300 m in the full resolution mode and about 1.2 km in the reduced resolution mode. Just as for MERIS, OLCI is optimised to monitor land surfaces, ocean colour over open oceans and coastal zones. Based on the excellent experience of the previous chosen MERIS channels, the MERIS channels have been kept. Importantly for atmospheric property retrievals, two additional bands, at 400 nm and 1020 nm, to improve atmospheric and aerosol correction capabilities, one additional band at 940 nm to better retrieve total column water vapour above dark surfaces have been added to the OLCI instrument. Of particular interest for cloud property retrievals are the two additional channels in the O_2 A-band for improving cloud top pressure retrievals. The latter two new channels, combined with the MERIS-like channels at 753 and 761 nm, and an additional window channel at 778.75, are used in the newly developed OLCI stand-alone algorithm as indicated by the red rows in Table 2-8.

Table 2-8 *OLCI spectral channels.*

Channel	Wavelength [nm]	Bandwidth [nm]
1	400	15
2	412.5	10
3	442.5	10
4	490	10
5	510	10
6	560	10
7	620	10
8	665	10
9	673.75	7.5
10	681.25	7.5
11	708.75	10
12	753.75	7.5
13	761.25	2.5
14	764.375	3.75
15	767,5	2.5
16	778.75	15
17	865	20
18	885	10
19	900	10
20	940	20
21	1020	40

OLCI data record used in Cloud_cci

Level 1b data of OLCI is used in Cloud_cci. Data identifier: OL_1_EFR; OL_1_ERR at Near Real Time (NRT).

2.7 Limitations of the (inter-)calibration

Inter-comparisons with MODIS-Aqua data concerning the three sensors AVHRR, AATSR and MERIS have shown good agreement for AVHRR and MERIS (i.e., deviation limited to 1-2 % for visible reflectances and as low as 0.1 % for infrared radiances). Larger deviations (up to 5 %) have been seen for AATSR. Because of limitations in the number of available inter-calibration targets (e.g., based on the SNO approach) as a consequence of the short period (three years) plus additional remaining uncertainties regarding effects for spectral differences (especially for AATSR), it has not been possible to firmly establish specific calibration corrections as an addition or complement to existing vicarious calibration corrections. For this reason and to evaluate potential trends, a longer evaluation period and access to improved spectral correction methods appear necessary.

3. Community retrieval algorithms

Two cloud property retrieval schemes are applied in Cloud_cci: FAME-C and CC4CL. The cloud properties derived by these schemes are listed in Table 1-2. Both schemes are briefly described in the following two subsections. In addition, Table 3-1 provides a fact sheet on important aspects of both schemes.

3.1 The Community Cloud retrieval for Climate (CC4CL) retrieval system

CC4CL consists of three main components: cloud detection, cloud typing and OE-based cloud property retrieval, which are summarized in the following subsections.

3.1.1 Cloud detection

The cloud detection is based on artificial neural networks (ANNs) that have been trained using AVHRR-NOAA-18 measurements and collocated CALIOP cloud optical depth (COD) for 12 days with optimal collocation conditions in 2008. The applied ANN outputs mimicked CALIOP COD (ANNCOD) in the range of 0 to 1. To convert the ANNCOD to a needed binary cloud decision, thresholds are applied which depend on illumination conditions (day/night/twilight) and region (land/sea). Verification scores were calculated, using the training data set, based on the ANNCOD output and the threshold applied, which are used to determine the uncertainty of the cloud mask decision per pixel. More information about the cloud detection can be found in ATBD-CC4CLv5.0 and Sus et al. (2017).

3.1.2 Cloud typing

Cloud typing is based on developments by Pavolonis and Heidinger (2004) and Pavolonis et al. (2005), which is based on a threshold decision tree. Cloud type output classes are:

- clear
- switched to water* (liquid)
- fog (liquid)
- water (liquid)
- supercooled (liquid)
- switched to ice* (ice)
- opaque ice (ice)
- cirrus (ice)
- deep convective (ice)
- overlap (ice)

The classes switched-to-water and switched-to-ice are additional classes introduced by Cloud_cci which account for too warm ice clouds (according to CTT) being reclassified to water and too cold liquid clouds being reclassified as ice. The cloud type information is then simplified to a binary cloud phase information (see phase of each class in brackets). More information about the cloud typing can be found in ATBD-CC4CLv5.0 and the references therein and in Sus et al. (2017).

3.1.3 Optimal estimation retrieval of cloud properties

The CC4CL retrieval of cloud properties is based on ORAC (Optimal Retrieval of Aerosol and Cloud) algorithm (Poulsen et al., 2012 and Watts et al., 1998, but including further developments made in the Cloud_cci Project: ATBD-CC4CLv5.0). The retrieval is based on the optimal estimation technique and can be used to determine both aerosol and cloud properties from visible/infrared satellite radiometers. In the case of cloud retrievals the algorithm, models the surface properties, atmosphere and subsequent fits the cloud properties using LUTs created from DIScrete Ordinates Radiative Transfer (DISORT) (Stamnes et al. 1998) to the TOA signal measured by the satellite by varying the cloud optical depth, effective radius, cloud top pressure, phase and surface

temperature. From these retrieved products we can subsequently derive liquid and ice water path. The optimal estimation framework of CC4CL provides some key advantages such as

- Comprehensive propagation of the measurement and forward model error into the final product.
- The ability to include prior knowledge of the retrieved quantities together with the uncertainties in a priori knowledge.
- A mathematically rigorous estimate of the uncertainty on retrieved values on a pixel by pixel basis by propagating the uncertainties of the measurements, model and a priori data.
- The retrieval also provides an indicator ('the cost') of the appropriateness of the model used.

A specific advantage of this algorithm is that it uses all channels and derives all parameters simultaneously. Hence the algorithm provides a measure of the consistency between retrieval representation of cloud and satellite radiance. The current version of CC4CL uses ORAC with RTTOV to calculate the clear sky radiances in the visible and infrared. The derived pixel level cloud properties are listed in Table 1-2, of which CTP, COT, CER are part of the state vector in the optimal estimation, while all others are derived. A summary is given in Table 3-1. More detailed information on the ORAC system can be found in ATBD-CC4CLv5.0.

3.1.4 Limitations

A full list of the assumptions and uncertainties are outlined in the uncertainty characterisation document (CECRv3). The main assumptions are listed below.

1. The CC4CL cloud algorithm as implemented within the Cloud_cci uses only the heritage channels.

2. The CC4CL cloud model assumes a single layer of cloud. No a priori climatological information is used in the retrieval to constrain the cloud heights hence the cloud height retrieved is the radiative effective cloud height in the case of multi layer clouds.

3. The CC4CL cloud retrieval uses the IR channels to assign the cloud height. The penetration depth of the IR clouds is approximately 1 optical depth into the cloud layer. The cloud height assignment and associated phase will be influenced by this, typically leading to a overestimation of the derived cloud top pressure (underestimation of cloud top height). An attempt to account for the semitranparency of many uppermost cloud layers is documented in Section 2.3.10 of ATBD-CC4CLv5.

4. The effective radius and optical depth retrievals are strongly dependent on the choice of optical properties used. The effective radius will differ for the 1.6 and 3.7µm retrievals if the vertical profile of effective radius changes with height. The 1.6µm channel penetrates deeper into the cloud.

3.2   The FUB AATSR MERIS Cloud (FAME-C) retrieval system

3.2.1   Collocation

A synergy product is generated using all AATSR and MERIS bands. This is done with an adapted version of the synergy tool developed at the University of Valencia (Gomez-Chova et al., 2009). The tool collocates the AATSR pixels on the MERIS grid, the resulting synergy product contains all AATSR and MERIS bands with a swath width of 493 pixels.

3.2.2   Cloud detection

A Bayesian cloud detection scheme is used as initial step. More information in Hollstein et al. (2015).

3.2.3   Cloud typing

The cloud typing and cloud phase determination is identical to CC4CL (see Section 3.1.2).

3.2.4   Optimal estimation retrieval of cloud properties

The FAME-C algorithm retrieves the cloud properties from top-of-atmosphere radiance measurements by MERIS and AATSR. Both instruments are mounted on the polar orbiting satellite ENVISAT (and accordingly OLCI & SLSTR on the future SENTINEL-3 satellite). It uses optimal estimation to provide error estimates (and pixel quality flags) on a pixel basis (Rodgers, 2000). A detailed description of the scheme is given in Carbajal Henken et al. (2014).

Three main steps can be identified. First, the cloud microphysical retrieval is performed for cloudy pixels to generate COT and CER daytime products. It is based on the DCOMP algorithm (Walther and Heidinger, 2012). In turn, a daytime LWP/IWP product can be computed. Second, the AATSR cloud height retrieval is performed to generate CTT products. Third, the MERIS cloud height retrieval is performed to generate CTP products. The microphysical cloud properties from the previous step are used as input in the cloud height retrieval.

All AATSR and MERIS Look-Up-Tables (LUTs) have been created using the radiative transfer model Matrix Operator Model (MOMO) developed at the Freie Universitaet Berlin (Fischer and Graßl, 1984; Fell and Fischer, 2001). For the retrieval of the AATSR CTT RTTOV 11.2 is used as the forward model.

3.2.5   Limitations

The synergetic FAME-C retrieval is currently only applicable during daytime. Since the cloud height retrieval step relies on information about the cloud microphysical properties that can be retrieved exclusively in the presence of sunlight, FAME-C is not applied on the night side of the earth.

The FAME-C cloud model assumes a single layer of cloud. In case of multi-layer clouds, the cloud height retrieved is the effective cloud height.

Since FAME-C is a fully synergetic retrieval, it can only be applied on the narrow AATSR swath with roughly 50% of MERIS swath remaining unused. This deficiency is avoided when applied to future observations of OLCI and SLSTR due to the equally wide swaths of these instruments.

In the current version of the retrieval, a cirrus cloud detection is applied in addition to the standard synergy cloud masking. This cirrus detection scheme is based on the split window brightness temperature difference of AATSR channels at 11µm and 12µm. In some cases, this procedure might result in classifying low level cloud edges as cirrus clouds, eventually resulting in an overestimation of the effective particle radius.

Table 3-1 *History of the community cloud retrieval schemes FAME-C and CC4CL*

	CC4CL	FAME-C
History	ORAC which was originally developed for application to SEVIRI (OCA, P. Watts). Applied to ATSR under nationally funded project GRAPE by RAL and University of Oxford	Building on earlier developments for retrieval of cloud-microphysical properties from AVHRR-like sensors (DCOMP, Walther and Heidinger, 2012) and cloud-top pressure from MERIS measurements (Preusker and Lindstrot, 2009).
COT CER	1. All cloud parameters retrieved simultaneously. NWP profiles calculated using RTTOV 2. Post correction of CTP/CTH for boundary layer inversion situations	After collocating MERIS and AATSR and performing cloud screening, COT and CER are retrieved from AATSR radiances (0.65μm, 1.6μm). MOMO RTM is used for producing LUTs.
CTP	3. Vis/NIR LUTS derived using DISORT RTM	CTP/CTT are retrieved from AATSR and MERIS measurements in the third and fourth step, taking COT and CER from step 2 as input. (CTT: 11μm, 12μm AATSR, CTP: 0.75μm, 0.76μm MERIS). RTTOV serves as forward model for the ATTSR 11 and 12μm BTs. MOMO is used for MERIS radiances.
LWP	$LWP = 4/3\ (\tau * re * \rho wat / Qwat)$; $Qwat = 2$ (τ: optical thickness, re: effective radius, ρwat: density liquid water)	$LWP = 2/3 * \tau * re * \rho wat$
IWP	$IWP = 4/3\ (\tau * re * \rho ice / Qice)$; $Qice = 2.1$ (τ: optical thickness, re: effective radius, ρice: density ice water)	$IWP = \tau * [(g0 * (1 + g1/g0) * (1/re)]^{-1}$; $g0 = 0.01256$; $g1 = 0.725$ (Heymsfield, 2003)
Ice	Baran Ice crystals	Baum Ice crystal data base (http://www.ssec.wisc.edu/~baum/)
Phase Discrimination	Done using cloud type analysis of Pavolonis et al. (2005), from which liquid and ice classes are aggregated.	Done using cloud type analysis of Pavolonis et al. (2005), from which liquid and ice classes are aggregated.
Cloud Mask	An ANN based retrieval is applied to all pixels and a pseudo CALIPSO COD threshold of 0.3 over land and 0.2 over sea is applied post hoc to flag cloud free and cloudy situations.	Cloud Mask is produced with a Bayesian cloud masking method (Hollstein et al. 2015).

	CC4CL	FAME-C
Snow/Ice discrimination	Snow and sea ice information is used from the NSIDC data base. Alternatively, ERA-Interim snow and ice information can be chosen. The information is used to modify the surface albedo.	MODIS snow/ice cover maps are used for better treatment of surface albedo and emissivity.

Errors
 	
Quality
Control
	Cost function provides an indication of the quality of the fit to the cloud model.
	
	If the fit is good then the errors indicate the accuracy of the retrieval.
	
	Convergence test: ORAC uses the change in the cost function between iterations to determine whether a retrieval is said to have converged.
	
	Errors considered
	
	    1. Measurement errors
	
	    2. Cloud inhomogeneity
	
	    3. Coregistraion error
	
	    4. Surface contribution
		Cost function provides an indication of the quality of the fit to the cloud model.
		
		If the fit is good then the errors indicate the accuracy of the retrieval.
		
		Convergence test: FAME-C uses the change in the cost function between iterations to determine whether a retrieval is said to have converged.
		
		Errors considered :
		
		1. Measurement errors
		
		2. Surface contribution
		
		3. Forward model parameter errors

Comments	Single layer plane parallel cloud assumed for all instruments. State vector also contains surface temperature.	Single layer plane parallel cloud assumed. Assumed vertical profile of volume extinction in cloud height retrieval depends on cloud type. Assumption based on analysis of global CloudSat measurements. No night retrieval at present.

4. Generation of the Level-3 products

The Cloud_cci data products are available at different processing levels including sensor-specific pixel level products (Level-2), sensor-specific global composites (Level-3U), sensor specific averaged products on a global grid (Level-3C), and merged, averaged products on a global grid (Level-3S). Details on the processing levels are reported in Table 1-3. All available Level-2 data are input to the Level-3 processing software.

The Level-3U/-3C/-3S grid is an equal angle grid covering the full globe. For the L3U sampled product the horizontal resolution is 0.05 degrees, while for Level-3C and Level-3S the spatial resolution is 0.5 degrees. The actual gridding is a straightforward process in which the latitude and longitude information of each L2 pixel is used to determine the indices of the corresponding grid cell the pixel falls into. This depends on the desired grid resolution.

The subsections below outline the averaging techniques applied for generation of the Level-3C data. The Level-3S data, which comprise the averages of sensor families and the averages of all sensors, are built by performing a weighted average of the individual sensor's Level-3C data.

4.1 Level-3U products

In order to reduce the amount of data and to map the data to a regular grid but without loosing all the horizontal variability by averaging it, a sampling technique has been implemented which is based on choosing the minimum satellite viewing zenith angle. This means that in the final product the pixel with the smallest satellite viewing zenith angle of all pixels falling into the grid cell is chosen to represent that grid cell. This is motivated by the fact that such a pixel is located closest to satellite nadir, which means that undesired effects due to a slant viewing path across the atmosphere are minimal. Since the footprint size increases with increasing satellite viewing angle, the grid cell that are covered by the footprint are calculated individually for each satellite pixel. This leads to that more than one grid cell can be filled with one individual observations depending on footprint size. Additionally, the L3U product is split up in ascending and descending satellite nodes. The viewing zenith angle sampling and the separation into the two nodes effectively leads to a larger temporal and spatial coherence of atmospheric patterns.

4.2 Level-3C/-3S products

4.2.1 Aggregating cloud mask and phase information

Cloud mask information consists of three stages: no information available (Fill value), clear (0) and cloudy (1). Averages are produced by counting the instances of clear and cloudy cloud mask information for each grid cell and evaluation of:

$$CC(i, j) = \frac{N(i, j)_{Cloudy}}{N(i, j)_{Cloudy} + N(i, j)_{Clear}}$$

4.2.2 Aggregating microphysical and macrophysical cloud properties

To ensure consistency when averaging the cloud properties, only those pixels are considered for which all cloud variables are available.. However, not for all cloudy pixels the cloud retrieval yields valid results, thus the pixels used for averaging cloud properties is usually a subset of those being identified as cloud (and used in the cloud fraction estimation). During night-time apparently no

consistence between micro and microphysical properties can be achieved due to the absence of microphysical retrievals.

The unweighted mean and standard deviation for grid cell (i,j) are then defined as:

$$< x(i,j) >= \frac{1}{N(i,j)_{Cloudy}} \sum_{k=1}^{N(i,j)_{Cloudy}} x_k(i,j)$$

$$s(x(i,j)) = (< x^2(i,j) > - < x(i,j) >^2)^{0.5}$$

Where i and j are the longitude and latitude indices. The error weighted mean and standard deviation for grid cell (i,j) are defined as:

$$< x(i,j) >_w = \frac{1}{W_1} \sum_{k=1}^{N(i,j)_{Cloudy}} x_k(i,j) w_k(i,j)$$

$$s(x(i,j))_w = (\frac{W_1}{W_1^2 - W_2} < x^2(i,j) >_w - < x(i,j) >_w^2)^{0.5}$$

With:

$$W_1 = \sum_{k=1}^{N(i,j)_{Cloudy}} w_k ; W_2 = \sum_{k=1}^{N(i,j)_{Cloudy}} w_k^2 ; w_k = \frac{1}{\sigma_k}$$

σ_k is the retrieval error of the corresponding variable. This approach is pursued for all micro- and macrophysical variables except for the cloud phase, for which, similar to the cloud cover, the number of liquid cloud instances per grid box is counted and

$$< cty(i,j) >= \frac{N(i,j)_{Cloudy}^{Liquid}}{N(i,j)_{Cloudy}}$$

is computed to give the liquid cloud phase contribution for grid box (i,j). Similar, the liquid and ice water paths are computed as:

$$< lwp(i,j) >= \frac{1}{N(i,j)_{Cloudy}^{Liquid}} \sum_{k=1}^{N(i,j)_{Cloudy}^{Liquid}} cwp_{liquid}$$

$$< iwp(i,j) >= \frac{1}{N(i,j)_{Cloudy}^{Ice}} \sum_{k=1}^{N(i,j)_{Cloudy}^{Ice}} cwp_{Ice}$$

Here, cwp_{Liquid} and cwp_{Ice} are distinguished by the cloud phase flag which is also used in counting the liquid and ice instances for $N(i,j)_{Cloudy}^{Liquid}$ and $N(i,j)_{Cloudy}^{Ice}$. These quantities are therefore connected by:

$$< cwp(i,j) >=< cty(i,j) >< lwp(i,j) > +(1- < cty(i,j) >) < iwp(i,j) >$$

Furthermore, to account for the special structure of the cloud top pressure for this variable the logarithmic average is computed additionally:

$$< ctp(i,j) >_{\ln} = \exp(\frac{1}{N(i,j)_{Cloudy}} \sum_{k=1}^{N(i,j)_{Cloudy}} \ln(ctp_k(i,j)))$$

Apart from those products referring to grid cell averages, 2D ISCCP-like histograms are also produced for each cell which partitions the CTP and COT space.
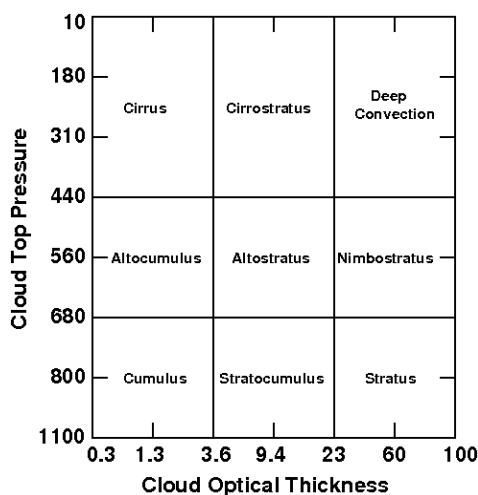

Figure 4-1 *ISCCP-like 2D cloud top pressure vs. cloud optical thickness histogram.*

The widths of the bins are defined as follows:

- COT: {0, 0.3, 0.6, 1.3, 2.2, 3.6, 5.8, 9.4, 15, 23, 41, 60, 80, 100}
- CTP: {1, 90, 180, 245, 310, 375, 440, 500, 560, 620, 680, 740, 800, 875, 950, 1100} [hPa]

As can be seen in Figure 4-1, this partitioning is also associated with nine different cloud types and thus allows for cloud classification of the grid cell.

In addition to the 2D histogram, also 1D histograms are generated for the parameters CTP, CTT, CWP, COT, CER. Each histogram covers the solution space of its variable with the cloud phase as additional dimension. These histograms are provided on the spatial resolution of the level3 averages. The used bins are:

- CWP: {0, 5, 10, 20, 35, 50, 75, 100, 150, 200, 300, 500, 1000, 2000, inf} [g/m^2]
- COT: {0.0, 0.3, 0.6, 1.3, 2.2, 3.6, 5.8, 9.4, 15.0, 23.0, 41.0, 60.0, 80.0, 100}
- CER: {0, 3, 6, 9, 12, 15, 20, 25, 30, 40, 60, 80} [µm]
- CTP:{ 1, 90, 180, 245, 310, 375, 440, 500, 560, 620, 680, 740, 800, 875, 950, 1100} [hPa]
- CTT:{ 200, 210, 220, 230, 235, 240, 245, 250, 255, 260, 265, 270, 280, 290, 300, 310, 350} [K].

5. Assumptions and limitations

5.1.1 Limitations in the aggregation of Level-3 products

Level 3 generation

As already stated in the text above, all Level-2 data of the month are regarded as equally valid and are summed up to derive the monthly means. Under certain circumstances this could lead to the monthly mean being biased towards days for which more Level-2 data are available compared to others. The applied approach is thus in contrast to weighting each day equally within a month, which on the other hand might lead to few, spatiotemporally isolated observations being overweighted. Under normal circumstances, under which the data coverage is nearly complete and nearly equally distributed within a month, the results of both approaches do no differ significantly.

Diurnal sampling

The diurnal cycle of clouds is well documented as a source of natural variability in the cloud field. It varies based on cloud type, latitude, season, and location. This cycle has significant effects on the horizontal and vertical distribution of clouds as well as on the cloud microphysical properties. The incomplete sampling of the diurnal cycle by polar orbiting satellite instruments, where usually 2 observations per day are taken for a specific place on Earth, introduces (1) differences between cloud data records of individual instruments when overpassing at significantly different local time, and (2) generally bias the cloud records compared to climatological means, for which more or less continuous observations within a day a required. By combining the records of the different sensors reduces the sampling error.

For proper interpretation of the temporal variability of individual Cloud_cci data records and among different records it diurnal cycle of cloud cover and possible methods to correct for it were assessed (RODCv1.0). However, Cloud_cci did not attempt to correct the cloud data records for the impact of the diurnal cycle, but rather provide the information. Corrections based on statistical analyses are inherently nonphysical and introduce uncertainty with little potential for information gain, however, they increase the stability of the time series.

6.   References

ATBD-FAME-Cv5, Algorithm Theoretical Baseline Document (ATBD) FAME-C – ESA Cloud_cci, Issue 5, Revision: 0, planned date of Issue: 12/09/2017, Available at: http://www.esa-cloud-cci.org/?q=documentation

ATBD-CC4CLv5, Algorithm Theoretical Baseline Document (ATBD) CC4CL – ESA Cloud_cci, Issue 5, Revision: 1, planned date of Issue: 28/07/2017, Available at: http://www.esa-cloud-cci.org/?q=documentation

Bodas-Salcedo, A., Webb, M.J., Bony, S., Chepfer, H., Dufresne, J.L., Klein, S.A., Zhang, Y., Marchand, R., Haynes, J.M., Pincus, R. and John, V.O., **2011**. COSP: Satellite simulation software for model assessment. Bulletin of the American Meteorological Society, 92(8), p.1023.

Bouvet M. , Adriaensen S., Barker K., Bourg L., Fougnie B., Govaerts Y., Henry P., Kent C., Smith D. and Sterckx S., "CEOS IVOS Working Group 4: Intercomparison of vicarious calibration methodologies and radiometric comparison methodologies over pseudo-invariant calibration sites", Report to CEOS IVOS, **2012**.

Carbajal Henken, C.K., Lindstrot, R., Preusker, R. and Fischer, J.: FAME-C: cloud property retrieval using synergistic AATSR and MERIS observations. Atmos. Meas. Tech., 7, 3873–3890, doi:10.5194/amt-7-3873-2014, **2014**

CECRv3, Comprehensive Error Characterization Report (CECR) – ESA Cloud_cci, Issue 3, Revision: 1, Date of Issue: 07/03/2017, Available at: http://www.esa-cloud-cci.org/?q=documentation

Donlon, C., B. Berruti, A. Buongiorno, M.-H. Ferreira, P. Femenias, J. Frerick, P. Goryl, U. Klein, H. Laur, C. Mavrocordator, J. Nieke, H. Rebhan, B. Seitz, J. Stroede, R. Sciarra, **2012**: The Global Monitoring for Environment and Security (GMES) Sentinel-3 mission. Remote Sens. of Environ., 120, 37-57

Fell, F., and J. **Fischer**, **2001**: Numerical simulation of the light field in the atmosphere-ocean system using the matrix-operator method. J. Quant. Spectrosc. Radiat. Transfer, 3, 351–388.

Feofilov, A. G., C. J. Stubenrauch, S. Protopapadaki, and R. Armante, **2017**: Diurnal variation of high-level clouds from a synergy of the space-borne infrared sounders AIRS and IASI: detection and radiative effects. In preparation for submission to ACPD.

Fischer, J., and H. **Grassl**, **1984**: Radiative transfer in an atmosphere-ocean system: An azimuthally dependent matrix-operator approach. Appl. Opt., 23, 1035–1039.

Gomez-Chova, L., Camps-Valls, G., Calpe, J., Munoz, J., and J. Moreno: MERIS/AATSR Synergy Algorithms for cloud screening, aerosol retrieval and atmospheric correction: Cloud Screening ATBD. University of Valencia, SYN-UV-ATBD 1.0, January **2009**

Heidinger, A.K., W.C. Straka, C.C. Molling, J.T. Sullivan and X.Q. Wu, **2010**: Deriving an inter-sensor consistent calibration for the AVHRR solar reflectance data record. Int. J. Rem. Sens.,31(24), 6493-6517.

Heymsfield, A.J., Matrosov, S. and Baum, B., **2003**. Ice water path–optical depth relationships for cirrus and deep stratiform ice cloud layers. Journal of Applied Meteorology, 42(10), pp.1369-1390.

Hollmann, R., Merchant, C.J., Saunders, R., Downy, C., Buchwitz, M., Cazenave, A., Chuvieco, E., Defourny, P., de Leeuw, G., Forsberg, R. and Holzer-Popp, T., **2013**. The ESA climate change initiative: Satellite data records for essential climate variables. Bulletin of the American Meteorological Society, 94(10), pp.1541-1552.

Hollstein, A., Fischer, J., Carbajal 5 Henken, C., and Preusker, R.: Bayesian cloud detection for MERIS, AATSR, and their combination, Atmospheric Measurement Techniques, 8, 1757–1771, doi:10.5194/amt-8-1757-2015, http://www.atmos-meas-tech.net/8/1757/2015/, **2015**.

Karlsson, K.-G.; **Johansson**, E. Multi-Sensor Calibration Studies of AVHRR-Heritage Channel Radiances Using the Simultaneous Nadir Observation Approach. Remote Sens. **2014**, 6, 1845-1862.

Lindstrot, R., Preusker, R. and Fischer, J., **2010**: The empirical correction of stray light in the MERIS oxygen A band channel, *J. Atmos. Oceanic Technol.*, 27 (7), 1185-1194.

McGarragh, G., Poulsen, C., Thomas, G., Povey, A., Sus, O., Schlundt, C., Stapelberg, S., Proud, S., Christensen, M., Stengel, M., and Grainger, R.: The Community Cloud retrieval for CLimate (CC4CL). Part II: The optimal estimation algorithm, submitted to Atmospheric Measurement Techniques Discussions, pp. –, **2017**.

Mittaz, P.D. and R. **Harris**, **2009**: A Physical Method for the Calibration of the AVHRR/3 Thermal IR Channels 1: The Prelaunch Calibration Data. J. Atmos. Ocean. Tech., 26, 996-1019, doi: 10.1175/2008JTECHO636.1

Pavolonis, M. J. and Heidinger, A. K.: Daytime cloud overlap detection from AVHRR and VIIRS, Journal of Applied Meteorology, 43, 762–778, **2004**.

Pavolonis, M. J., Heidinger A. K., and Uttal, T., Daytime Global Cloud Typing from AVHRR and VIIRS: Algorithm Description, Validation, and Comparisons, J. Appl. Meteor., 44, 804-826, doi:10.1175/JAM2236.1, **2005**.

Poulsen, C.A., Siddans, R., Thomas, G.E., Sayer, A.M., Grainger, R.G., Campmany, E., Dean, S.M., Arnold, C. and Watts, P.D., **2012**. Cloud retrievals from satellite data using optimal estimation: evaluation and application to ATSR. *Atmospheric Measurement Techniques*, 5(8), pp.1889-1910.

Preusker, R., and R. **Lindstrot**, **2009**: Remote sensing of cloud-top pressure using moderately resolved measurements within the oxygen A band—A sensitivity study. J. Appl. Meteor. Climatol., 48, 1562–1574.

PUGv3.1, Product User Guide (PUG) – ESA Cloud_cci, Issue 3, Revision: 1, Date of Issue: 18/04/2017, Available at: http://www.esa-cloud-cci.org/?q=documentation

PVIRv4.1, Product Validation and Intercomparison Report (PVIR) – ESA Cloud_cci, Issue 4, Revision: 1, Date of Issue: 18/04/2017, Available at: http://www.esa-cloud-cci.org/?q=documentation

RAFCDRv1.0, Technical Report on AVHRR GAC FCDR generation – ESA Cloud_cci, Issue 1, Revision: 0, planned date of Issue: 06/2017. Available at: http://www.esa-cloud-cci.org/?q=documentation

RODCv1.0, Report on Orbital Drift Correction for AVHRR – ESA Cloud_cci, Issue 1, Revision: 0, planned date of Issue: 06/2017. Available at: http://www.esa-cloud-cci.org/?q=documentation

Rodgers, C.D. , **2000**: Inverse methods for atmospheric sounding, World Scientific Publishing Pte Ltd, New York, USA.

Smith, D. L., Delderfield, J., Drummond, D., Edwards, T., Mutlow, C. T., Read,P. D., and Toplis, G. M.: Calibration of the AATSR Instrument, Adv. Space Res., 28(1), 31--39, **2001**.

Smith, D., Poulsen, C., and Latter, B.: Calibration status of the AATSR reflectance channels, 2008 ESA MERIS/(A)ATSR Workshop, **2008**.

Stamnes K., Tsay S.C., Wiscombe W. and Jayaweera K., **1998**: Numerically stable algorithm for discrete ordinate method radiative transfer in multiple scattering and emitting layered media, Appl. Opt., 27, 2502-2509.

Stengel, M., Stapelberg, S., Sus, O., Schlundt, C., Poulsen, C., Thomas, G., Christensen, M., Carbajal Henken, C., Preusker, R., Fischer, J., Devasthale, A., Willén, U., Karlsson, K.-G., McGarragh, G. R., Proud, S., Povey, A. C., Grainger, D. G., Meirink, J. F., Feofilov, A., Bennartz, R., Bojanowski, J., and Hollmann, R.: Cloud property datasets retrieved from AVHRR, MODIS, AATSR and MERIS in the framework of the Cloud_cci project, Earth Syst. Sci. Data Discuss., https://doi.org/10.5194/essd-2017-48, in review, **2017**.

Stubenrauch, C. J., A. G. Feofilov, S. E. Protopapadaki, R. Armante, **2017**: Cloud climatologies from the InfraRed Sounders AIRS and IASI: Strengths, Weaknesses and Applications In preparation for submission to ACPD

Sus, O., Jerg, M., Poulsen, C., Thomas, G., Stapelberg, S., McGarragh, G., Povey, A., Schlundt, C., Stengel, M., and Hollmann, R.: The Community Cloud retrieval for CLimate (CC4CL). Part I: A framework applied to multiple satellite imaging sensors, submitted to Atmospheric Measurement Techniques Discussions, pp. –, **2017**.

Walther, A. and Heidinger, A.K., **2012**. Implementation of the daytime cloud optical and microphysical properties algorithm (DCOMP) in PATMOS-x. *Journal of Applied Meteorology and Climatology*, *51*(7), pp.1371-1390.

Watts P.D., Mutlow C.T., Baran A.J. and Zavody A.M., **1998**: Study on cloud properties derived from Meteosat Second Generation Observations. Eumetsat Report, http://www.eumetsat.de/en/area2/publications/rep_cloud.pdf.

7. Glossary

AMSR-E	Advanced Microwave Scanning Radiometer-EOS
AATSR	Advanced Along Track Scanning Radiometer
AM	Ante Meridiem
AVHRR	Advanced Very High Resolution Radiometer
BRDF	Bidirectional Reflectance Distribution Function
BT	Brightness Temperature
Calipso	Cloud-Aerosol Lidar and Infrared Pathfinder Satellite Observation
CFC	Cloud Fractional Coverage
CLOUDSAT	Cloud-Aerosol Lidar and Infrared Pathfinder Satellite Observations
CM SAF	EUMETSAT Satellite Application Facility on Climate Monitoring
CMUG	Climate Modelling User Group
CPH	Cloud Phase
COT	Cloud Optical Thickness
CTH	Cloud Top Height
CTP	Cloud Top Pressure
CTT	Cloud Top Temperature
DISORT	Discrete Ordinates Radiative Transfer
ECMWF	European Centre for Medium-Range Weather Forecasts
ECV	Essential Climate Variable
ENVISAT	Environmental Satellite
EOS	Earth Observing System
ESA	European Space Agency
FAME-C	FUB AATSR MERIS Cloud retrieval algorithm
FCDR	Fundamental Climate Data Record
GAC	Global Area Coverage – globally available AVHRR dataset with reduced resolution (4 km).
GSICS	Global Space-based Inter-Calibration System
GCOS	Global Climate Observing System
GEWEX	Global Energy and Water Cycle Experiment
JCH	Joint Cloud property Histogram
ISCCP	International Satellite Cloud Climatology Project
IWP	Ice Water Path
K	Kelvin

KNMI	Koninklijk Nederlands Meteorologisch Instituut
LUT	Look-up Table
LWP	Liquid Water Path
MERIS	Medium Resolution Imaging Spectrometer
MetOp	Meteorological Operational Satellite
MODIS	Moderate Resolution Imaging Spectroradiometer
MOMO	Matrix Operator Model
NASA	National Aeronautics and Space Administration
NCDC	National Climatic Data Center
NSIDC	National Snow and Ice Data Center
NOAA	National Oceanic & Atmospheric Administration
OLCI	Ocean Land Colour Instrument
ORAC	Oxford RAL Aerosol and Cloud Algorithm
PATMOS-x	AVHRR Pathfinder Atmospheres - Extended
PM	Post Meridiem
CER	Effective Radius
RTTOV	Radiative Transfer for (A)TOVS
SEVIRI	Spinning Enhanced Visible and Infrared Imager
SNO	Simultaneous Nadir Overpass
SMHI	Swedish Meteorological and Hydrological Institute
SLSTR	Sea and Land Surface Temperature Radiometer
TCDR	Thematic Climate Data Record
TOA	Top Of Atmosphere